

Single Electron Detection in Quadruple-GEM Detector with Pad Readout.

J. Va'vra,

Stanford Linear Accelerator Center, Stanford University, Stanford, CA 94309, U.S.A.

A. Sharma¹

University of Maryland, College Park, 20742 MD, USA

Abstract

Using a system of four GEMs operating in tandem and coupled to pad readout, we have demonstrated the detection of single electrons in ethane at 1 bar. The paper presents measurements of single electron pulse height distributions, total gas gain measurement and calculation, pad-to-pad cross-talk, quenching capability, high rate capability, charging effects, etc. We describe the overall operational experience, including addition of a gaseous photocathode, TMAE, and compare it to the SLD CRID single-electron detector [1], which has been operational during the past decade.

1. INTRODUCTION

The Gas Electron Multiplier (GEM) has been introduced by F. Sauli [2], and it has quickly become a source of interest in the detector field. Coupled to a second amplification and read-out device, such as MWPC, MSGC (MicroStrip Gas Chamber), or another GEM with a simple PC-board, it has already been demonstrated that the GEM electrode can work reliably.

Until recently, there were relatively few attempts to use the GEM for applications trying to detect single electrons such as the Cherenkov particle identification detectors. For example, J. Seguinot has built a photon detector with a combination of the MSGC and the GEM with a CsI photocathode operating at normal pressure [3]. A. Breskin et al. have tried a single-GEM coupled to a MWPC operating at low pressure [4], and similarly, one of us (JV) has tried a single GEM coupled to a MWPC operating in ethane at normal pressure [5].

It has been demonstrated, using calculations with the 3D-MAXWELL and GARFIELD computer programs, that coupling of a MWPC to the GEM foil reduces the GEM's exit electric field, which in turn reduces the "exit charge efficiency," which can be as low as 20-40% [6]. The preferred solution is to couple the GEM to pad readout. This has been shown as possible in the calculation [7], and as well as experimentally by Breskin's group, which has tried recently the single electron detection with 3 and 4 GEM system with pad readout [8,9], where the entire GEM electrode is one single pad. This enhances the coupling efficiency compared to coupling to many small pads with aim to determine the position of the avalanche.

We have decided to pursue the coupling of four GEMs to pad readout. We believe that this is the first practical attempt to use this particular configuration to detect single electrons. The reason for four GEMs was to

¹ Mailing address CERN CH 1211, Geneva, Switzerland.

reduce the gas gain load per GEM to absolute minimum, thus permitting reliable operation even in hydrocarbon gases, such as ethane at 1 bar. In principle, it is possible to consider even higher number of GEMs in future.

Any single electron sensitive detector has to survive a blast of background ionization due to various sources such as beam dumps, heavy ions, muons aligned with the TPC axis (SLD CRID experience), etc. For example, in the last example, one is dealing with more than 10^4 primary electrons arriving on one spot of the detector within $\sim 30\mu\text{s}$, a non-trivial number by any means. A repetitive background can also contribute to the Kapton charging effects, which could also enhance the gas gain locally. It is difficult to simulate such background sources in the lab. We have used a high intensity UV lamp to simulate a background and the charging effects.

The motivation for this work was a possibility that SLD might extend the run to collect one million Z 's with upgraded SLC in 1998. The idea was to see if it would make sense to replace the existing CRID detectors [1] with a novel type, while keeping the rest of TPCs as they are. Although the possibility of such a run is now remote, we have nevertheless developed the prototype and report on its results.

2. DESIGN OF THE DETECTOR AND THE EXPERIMENTAL SETUP

The concept of the prototype is described in Fig. 1. The GEM foil was manufactured at the CERN Surface Treatment workshop and provided to us by F. Sauli. It consists of a thin Kapton foil ($\sim 50\mu\text{m}$ thick) sandwiched between two metal layers ($\sim 18\mu\text{m}$ thick copper), pierced by a regular matrix of holes, which are created using high-precision wet etching process. The GEM double conical hole pattern has a pitch of $120\mu\text{m}$, the Kapton hole diameter is $40\mu\text{m}$, and the copper hole diameter is $80\mu\text{m}$. The GEM size was $\sim 13 \times 1.5$ cm, although the active region was only $\sim 122\text{mm}^2$ in this test. The readout pads are circular 1.25 mm in diameter and with 2.5 mm pitch. The pad plane is 0.8 mm away from the last GEM. The operating voltages and the resistor chain values are shown in Table 1. In this design, we have graduated dV_{gem} voltages to have the smallest gain in the GEM closest to the pads, where the anode current is largest and so is the possible charging effect.

We use the SLD CRID charge amplifier with a gain of $\sim 2.7\mu\text{V}/\text{electron}$ and a shaping time of 65ns and $\sigma_{\text{Noise}} \sim 2100$ electrons. The idea was to keep the same electronics when the run at SLD was considered. However, such a short shaping time constant forces the detector to operate at a rather high average visible gas gain of $\sim 2 \times 10^5$, because the total gain, which is corrected for various charge losses in the four GEM system is even higher ($\sim 5 \times 10^5$). Conclusions of this test will be relevant for the LHC or HERA-b applications, where similar short shaping time constants are required. However, since we do have the pad readout, and relatively low rates, it is possible to consider the shaping time of about $\sim 1\mu\text{s}$, which would allow to reduce the gas gain to $\sim 2-3 \times 10^4$, as has been demonstrated by the ALICE and CLEO RICH experiments. This would considerably improve the robustness of the presented detector.

It is assumed that in the final application, for example for the SLD CRID, one would tie pads resistively together into 10cm-long columns, each having a resistivity of $\sim 40\text{k}\Omega$, to be able to utilize the existing CRID charge division readout electronics. However, in this test, we kept the pads independent. The very first GEM, facing the TPC drift volume, would see an electric field of $\sim 400\text{V}/\text{cm}$, which would provide a full entrance electron transfer efficiency, according to our simulation, as shown in Fig. 2.

Our gas system, just like the one at SLD, used stainless steel tubing, Oxisorb and Molecular sieve filters to purify the gas to a level of <1ppm of oxygen and ~5ppm of water. We have chosen a single component gas, ethane, which gave excellent results at SLD CRID. In this test, we actually used ethane gas from SLD CRID², which is very pure by itself. By choosing the very pure gas, we may have provided excellent conditions for the GEM electrode charging, which may not exist in a typical lab setup.

3. EXPERIMENTAL RESULTS

Figures 3-6 show several examples of experimental results with this detector, which demonstrate the capability of single electron detection. The detector used ethane gas at 1 bar and room temperature. Figure 3 shows typical single electron pad pulses in ethane gas at $V_{top} = -5.5$ kV. See Table 1 for the distribution of GEM voltages. In this case, the single electrons are created by UV light striking the mesh under the window (Fig. 1). Triggering on the photodiode signal, one sees that the probability that a pad has a signal is a few percent only, which ensures that we are indeed dealing with the single electrons. Figure 4 shows single electron pulse height spectrum in ethane at $V_{top} = -5.7$ kV, together with the electronics calibration peaks obtained by injecting a known charge into the amplifier through a 1.2pF capacitor. The scale represents the visible gain, i.e., the signal observed by an amplifier, i.e., it is not corrected for the GEM system charge losses. Figure 5 shows the pedestal together with the single electron pulse height spectrum, which can be fitted well with an exponential function. The only way to show the small pulse height region in the vicinity of the pedestal, and also to see directly a probability of having the single electron pulse, is to use the external trigger to QVT provided by the photodiode signal. There is no excess in the large pulse height region, which is a sign of good quenching and stable operation [11]. Figure 6 shows that the cross-talk from the signal pad to its nearest neighbor pad is at a level of 1-2%.

Figures 7 and 8 show behavior of the detector under the high current condition. Figure 7 shows the total gas gain as a function of V_{top} measured using the total current method. To do this measurement, all pads were connected together to the Keithley 485 pico-ammeter. The gain is calculated as a ratio of the anode current at a given V_{top} voltage normalized to the anode current at $V_{top} \sim -1$ kV, which is a voltage at which the detector has no gas gain. To avoid charging at large amplified anode currents, we have chosen as small incident photon flux as possible, yielding the total anode current of only $I(V_{top} = -1 \text{ kV}) \sim 2.2$ pA (see Fig. 8), which corresponds to a very small total anode current density of $N_a \sim 0.018$ pA/mm², or $\sim 1.1 \times 10^5$ photoelectrons/(sec.mm²). For these conditions, we have reached the total visible gas gain close to $\sim 10^6$. Figure 7 shows also our calculation of the total visible gas gain in ethane at 1 bar, based on the model prepared using 3D-MAXWELL³ and GARFIELD⁴ computer programs [6]. Table 2 shows the computer simulated distribution of the charge flow through various detector segments in this particular design in ethane at $V_{top} = -5.5$ kV. We have repeated this measurement a number of times and the GEM foils were never damaged, when operating in ethane gas. At this point, we introduced a small amount of TMAE by bubbling ethane through a 15°C liquid TMAE. The total anode current increased to $I(V_{top} = -1 \text{ kV}) \sim 750$ pA (see Fig. 8), corresponding to the total anode current density of

² Purchased from AlphaGaz Co., with purity specification 99.995%.

³ Commercial Finite Element Analysis Computer Program, Ansoft SA, Pittsburgh, PA, USA.

⁴ Drift Chamber Field and Performance Computation Program, R. Veenhof, CERN.

$N_a \sim 6.2 \text{ pA/mm}^2$. The gain became larger for a given V_{top} and steeper compared to the low photon flux condition in ethane, but more importantly, we have permanently damaged three out of four GEM foils already at $V_{\text{top}} \sim 3 \text{ kV}$. All three GEMs developed a finite resistivity of few $\text{M}\Omega$, and one may suspect a carbonization path on the Kapton surface coated with TMAE, caused by a discharge. At the point of damage, the total anode current was only $\sim 360 \text{ nA}$, the total anode current density was $N_a \sim 3 \text{ nA/mm}^2$, or $\sim 3 \times 10^8$ electrons/sec/(single hole in the last GEM). We can use this result to predict the maximum allowable incident photoelectron rate in ethane + TMAE gas, assuming that the detector is in the single electron mode with the total gain of $\sim 5 \times 10^5$. Assuming that the “Total Anode Current” \equiv “Total Gain” * “Entrance Photoelectron Current,” then the total anode current of $\sim 360 \text{ nA}$ is equivalent to the entrance photoelectron rate of $\sim 4 \times 10^4$ el./sec/ mm^2 . Therefore, a safe limit for a typical practical operation is probably only few kHz/mm^2 (safety factor of 10 guarding against unforeseen breakdowns, beam dumps, etc.). One would improve the robustness of the detector further by lowering the total gas gain to $\sim 2 \times 10^4$, which could be, perhaps, achieved by reducing the electronics noise using either a better electronics or by increasing the shaping time constant.

Since the GEM damage was a significant event, and furthermore the Kapton charging can affect the gas gain, we have decided to investigate the charging effects in more detail in the following chapter. Only two-damaged GEM foils could be cured with the alcohol and an ultrasonic bath, the third one had to be replaced. The new stack with a new GEM foil had somewhat lower gain (affects the results in remaining part of the paper).

4. OBSERVATION OF CHARGING EFFECTS IN THE QUADRUPLE-GEM DETECTOR

The GEM electrode contains the Kapton material, which is a very good insulator, if it is kept in low humidity conditions. In addition, we have not compared the conical holes in our GEM foils with other possible designs, for example, to the cylindrical holes [12,13]. Furthermore, we have not coated the surfaces to increase their conductivity [14]. We describe the charging effects in a system of four GEMs in this section.

Some fraction of the positive ions generated during the amplification process within the GEM hole may drift towards the Kapton walls, and stay there some time before they are neutralized with a certain discharge time constant. We have decided to measure this time constant by measuring the time dependency of the “remnant” anode current immediately after the UV lamp was switched off. To do this measurement, the quadruple-GEM detector was set to the charge collection mode at certain V_{top} voltage, and then the anode current was followed immediately after switching the lamp off. Figure 9 shows the results for two V_{top} values of -4 and -4.5 kV, which indicate that the discharge time constant is about one-minute. Figure 10 shows that the remnant currents are less than 1% of the total anode current prior to switching the light off within less than one second. We obtained very similar results with ethane prior to introduction of TMAE, i.e. TMAE is not a factor.

Similarly, one would expect that a build up of positive charge on the Kapton surface would create two effects: (a) a slow gain increase, and (b) change of the electric field in the exit of the GEM hole. We have decided to investigate the charge build up by following the anode current immediately after switching the UV lamp on. Again, this process has a certain charging time constant. To do this the quadruple-GEM detector was set to the charge collection mode at a certain V_{top} voltage. The incident UV light was switched on by a shutter

rather than switching the lamp on. Figure 10 shows the charging response for different V_{top} voltages. One can see that the charging up time constant is consistent with that of the “remnant” current measured in Fig. 9. A consequence of the charging effects is that one has to wait 2-3 minutes before the anode current is stabilized.

One should say that all above measurements were done at extremely low humidity (~ 5 ppm). We have decided to measure the charging up effects as a function of humidity. Figure 11 indicates that there is some hint of shortening the charging time constant if we approach the humidity level of 200ppm. TMAE can live with some humidity, although 200ppm is probably too high a value.

As the incident photon flux increases, one expects a buildup of the gas gain due to the charging of Kapton. Figure 12 shows that we do not see any effect up to the total anode currents of ~ 16 pA, which corresponds to anode current density of 0.14 pA/mm². The analysis of charging effects at larger currents is in progress.

The charging tests described in this chapter were done at a relatively high photon flux ranging between $\sim 10^4$ to $\sim 4 \times 10^8$ photons/(sec.mm²). Such a large flux is not typically found in any experiment. For example, the DIRC photon detector, which operates at the high luminosity experiment BaBar, detects typically less than 100-background photons/(sec.mm²) striking a PMT. Similarly, the SLD CRID environment can be considered as low background. However, one cannot avoid occasional highly ionizing events depositing the charge locally in rapid sequence.

5. COMPARISON OF EXPERIENCE WITH THE CRID DETECTOR

The CRID detectors operated successfully with TMAE gas in the SLD experiment for about 10 years, and it is therefore useful to compare the relative experience. These detectors used a $7\mu\text{m}$ diameter high resistive ($\sim 40\text{k}\Omega$) carbon anode wire. The non-linear gain response of thin anode wires to large charges as well as the wire resistance were the main reason for the operational stability. On the other hand, the $7\mu\text{m}$ carbon wire does not provide a long term mechanical resiliency, which caused occasional wire breakage.

The behavior of the quadruple-GEM detector with pad readout provided almost the same feel as that of the CRID detector in terms of the single electron detection operational behavior, while the CRID MWPC detectors were more tolerant to over-voltage. The quadruple-GEM detector behaved better than a combination of MWPC and a single GEM reported by us earlier [4]. Certainly, the most attractive feature of the detector presented in this paper is absence of wires.

6. CONCLUSION

We have demonstrated a successful operation of the quadruple-GEM detector with the pad readout in the single electron mode. However the paper also expresses a word of caution regarding use of this type of detector, as presented in this paper, in the high background environment. The GEM can be damaged in ethane + TMAE gas if the entrance photoelectron rate exceeds $\sim 4 \times 10^4$ el./sec/mm², and the detector is operating at the average visible gain of $\sim 2 \times 10^5$. In this case, a safe limit for a typical practical operation is probably few kHz/mm² (assuming a safety factor of ten for possible beam dumps, sparks, etc.). We also strongly recommend, if it is possible in a given application, to reduce the electronics noise through either a better electronics or by increasing the shaping time, which would allow lowering of the total gas gain to $\sim 2 \times 10^4$. Clearly, many variables have to be still tuned before this concept can be used in a large application.

ACKNOWLEDGEMENTS

We would like to thank F. Sauli for providing the CERN-made GEM electrodes and comments to this text. We also thank M. McCulloch for help to construct the quadruple-GEM detector.

REFERENCES

1. K. Abe et al., Nucl. Instr. & Meth., A343 (1994) 74, and J. Va'vra, Nucl. Instr. & Meth., A433 (1999) 59.
2. F. Sauli, Nucl. Instr. & Meth., A386 (1997) 531, and R. Bouclier et al., IEEE Trans. Nucl. Sci., NS-44 (1997), 646.
3. J. Seguinot and T.Y. Ypsilantis, Nucl. Instr. & Meth., A433 (1999) 1-16.
4. R. Chechik et al., Nucl. Instr. & Meth., A419 (1998) 423.
5. J. Va'vra, G. Manzin, M. McCulloch, P. Stiles and F. Sauli, Nucl. Instr. & Meth., A433 (1999) 527.
6. A. Sharma, "3-D Simulation of Charge Transfer in a GEM and Comparison to Experiment," Presented at the SAMBA Symposium, Siegen, Germany, October 1999, Nucl. Instr. & Meth. A 454(2000)267.
7. A. Sharma, To Appear in Proceedings, Medical Imaging Conference, Stockholm, Sweden, October June 2000, CERN-EP 2000-145.
8. A. Buzulutskov, A. Breskin, R. Chechik, G. Garty, F. Sauli and L. Shekhtman, Nucl. Instr. & Meth., A443 (2000) 164-180.
9. A. Buzulutskov, A. Breskin, R. Chechik, G. Garty, F. Sauli and L. Shekhtman, Nucl. Instr. & Meth., A442 (2000) 68-73.
10. Bressan et al., Nucl. Instr. & Meth., A423 (1999) 119.
11. J. Va'vra, Nucl. Instr. & Meth., A371 (1996) 33.
12. J. Benlloch, A. Bressan, M. Capea'ns, M. Gruwe', M. Hoch, J.C. Labbe', A. Placci, L. Ropelewski, F. Sauli, Nucl. Instr. & Meth., A419 (1998) 410, and references therein.
13. K. Pitts et al., To appear in Proceedings of the IEEE Conference on Nuclear Physics and Imaging, Lyon, France, October 2000.
14. G. Zech, Private communication.

Table 1: Quadruple-GEM voltages for $V_{\text{top}} = -5.5$ kV, where the single electron sensitivity was obtained. Notice that the highest voltage of the GEM stack is about $V_8 = -4.25$ kV for $V_{\text{top}} = -5.5$ kV, and a typical voltage across four GEMs is ranging from -435 V to -594 V, the lower number corresponding to the GEM closest to the pads.

Resistors	[Mohms]	Voltages	[V]	dV	[V]
R1	7	V1	417.5	dV1	417.5
R2	7.29	V2	852.4	dV2	434.8
R3	9.91	V3	1444	dV3	591.1
R4	8.01	V4	1921	dV4	477.8
R5	10.02	V5	2519	dV5	597.7
R6	9.03	V6	3058	dV6	538.6
R7	9.98	V7	3653	dV7	595.3
R8	9.96	V8	4247	dV8	594.1
R9	0.996	V9	4306	dV9	59.41
R10	10.04	V10	4905	dV10	598.9
R11	9.97	Vtop	5500		

Table 2: Computer simulation of the charge losses and transmission accounting in the quadruple-GEM detector at $V_{\text{top}} = -5.5$ kV (see Table 1 for voltage distribution). GEM 1 is closest to the pad electrodes.

Variable	GEM 1	GEM 2	GEM 3	GEM 4
Ions charge ending at the top GEM electrode [%]	6	4	5	6
Ions charge ending on the Kapton insulator [%]	2	3	3	6
Electron charge ending at the top GEM electrode [%]	15	10	12	5
Electron charge ending on the Kapton insulator [%]	1	3	5	15
Electron charge ending at the bottom GEM electrode [%]	20	26	28	32
Transmitted electron charge [%]	56	54	47	36

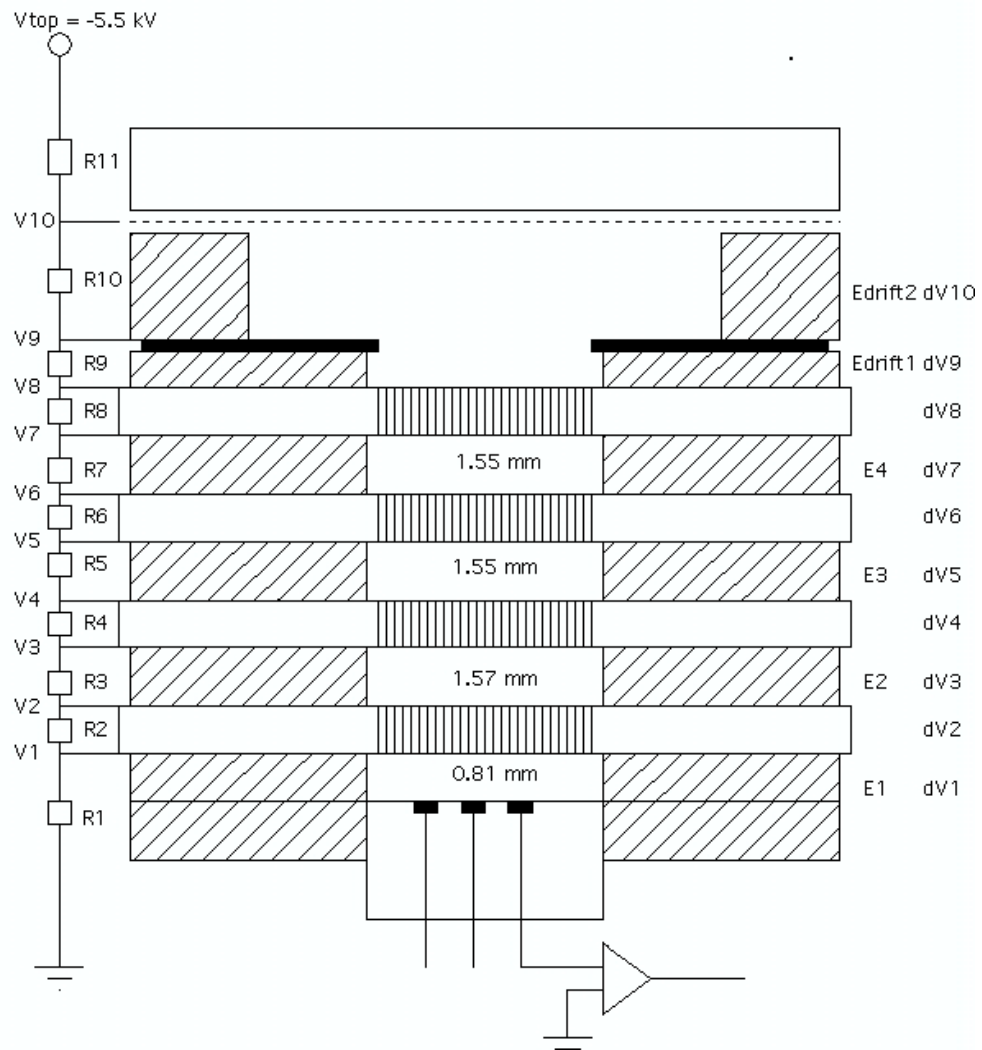


Fig.1. Quadruple-GEM detector with pad readout used in this test.

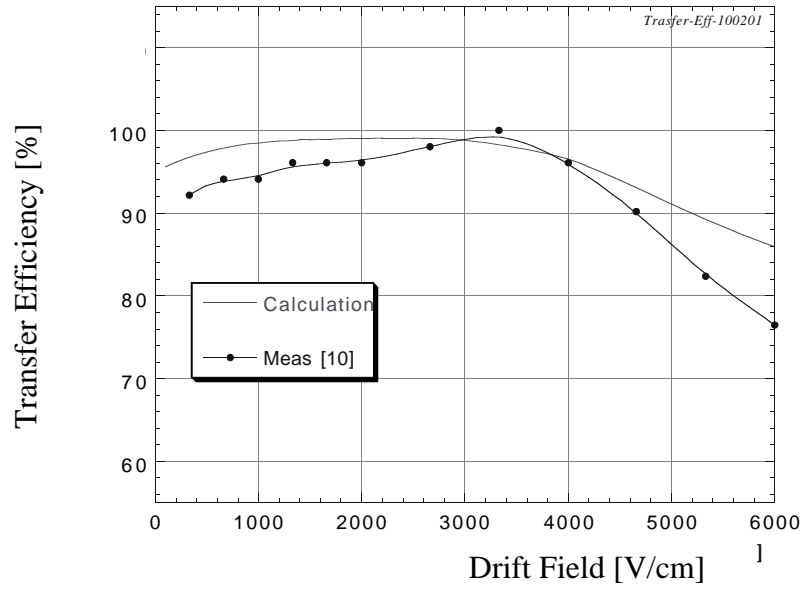


Figure 2. Calculation of transfer efficiency of single electrons from the drift region across the first GEM with $dV_{\text{gem}} = 500\text{V/cm}$. The data came from Ref. 10.

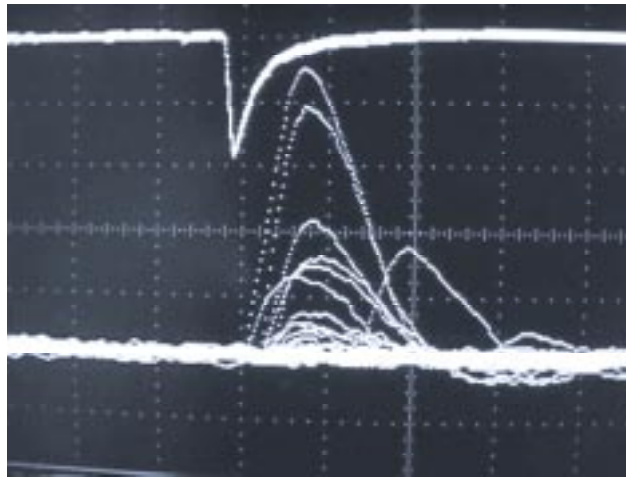


Fig.3. Typical single electron pulses from pads (bottom trace; 50mV/div , 200ns/div) in ethane at $V_{\text{top}} = -5.5\text{ kV}$, together with a photodiode pulses (top trace) used to trigger the scope. The single electrons are created by UV light striking the mesh under the window – see Fig. 1.

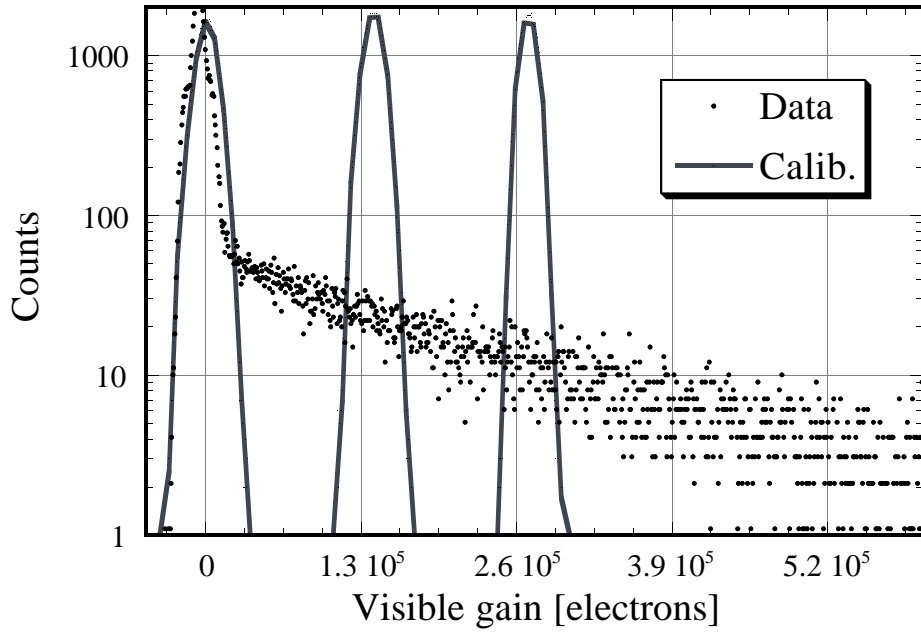


Figure 4. Single electron pulse height spectrum in ethane at $V_{\text{top}} = -5.7$ kV, together with the electronics calibration of the visible gain obtained by injecting a known charge into the amplifier.

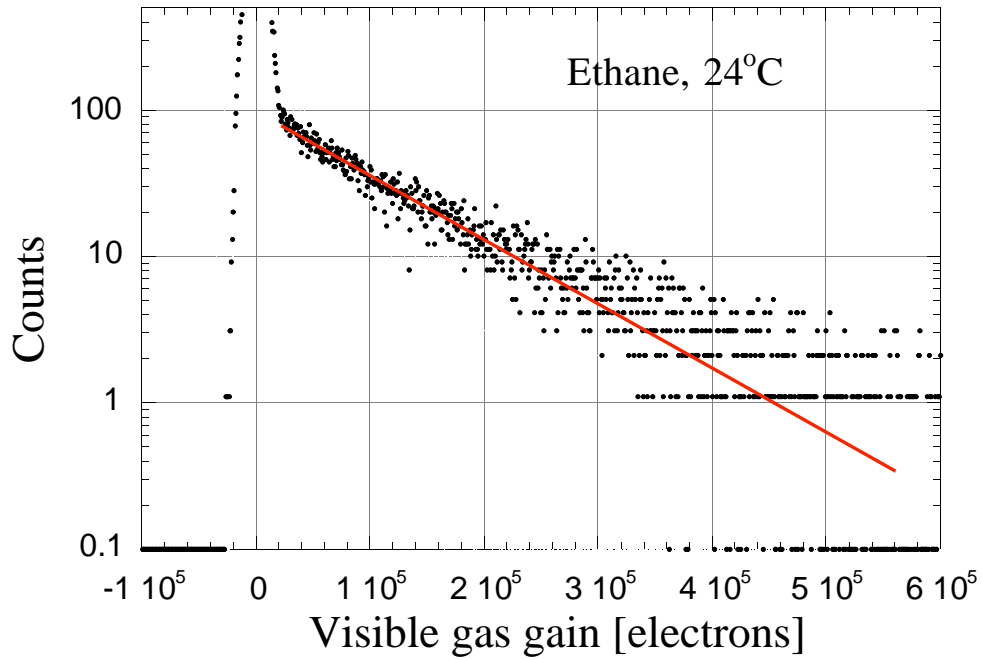


Figure 5. Single electron pulse height spectra in ethane at $V_{\text{top}} = -5.6$ kV. The external trigger to QVT is provided by the photodiode signal. The pulse height spectra is close to exponential. The gas was ethane at 1 bar and room temperature.

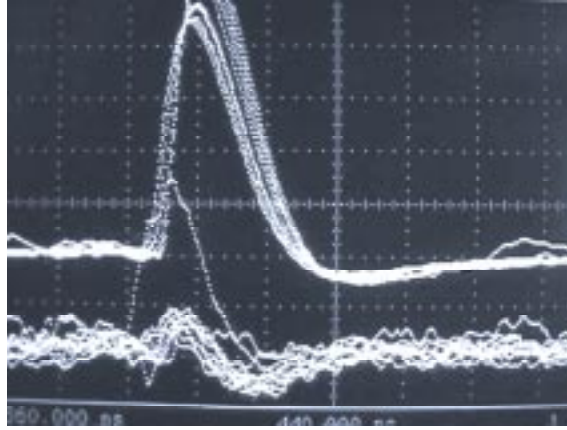


Figure 6. The cross-talk from pad to pad is at a level of 1-2%. Signal pad (top trace: 100mV/div), neighbor pad (bottom trace: 20mV/div), time scale is 200ns/div. The gas was ethane at 1 bar and room temperature.

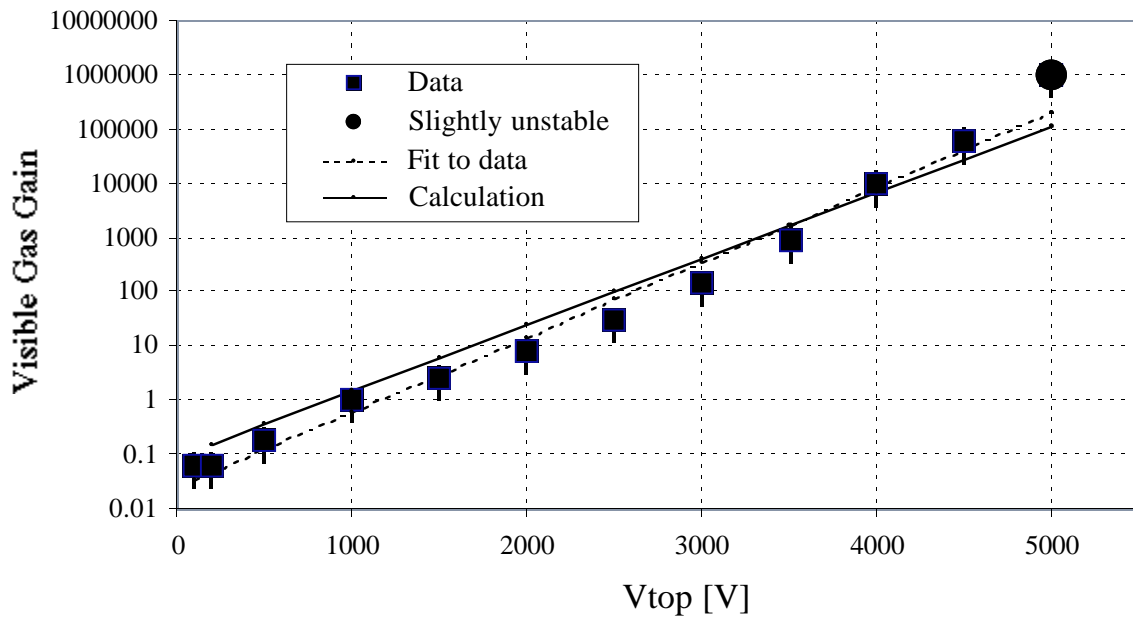


Figure 7. The visible gas gain data in ethane at 1 bar as a function of V_{top} (black squares). The anode current at no gas gain condition was chosen as small as possible, i.e., $I(V_{top} \sim 1\text{kV}) \sim 2.2\text{pA}$, which corresponds to the anode density of about $N_a \sim 0.018\text{pA/mm}^2$. Under this condition, we reach the visible gas gain close to $\sim 10^6$ at $V_{top} \sim 5\text{kV}$. The graph shows also a fit to data and a calculation using the 3D-MAXWELL and GARFIELD computer programs.

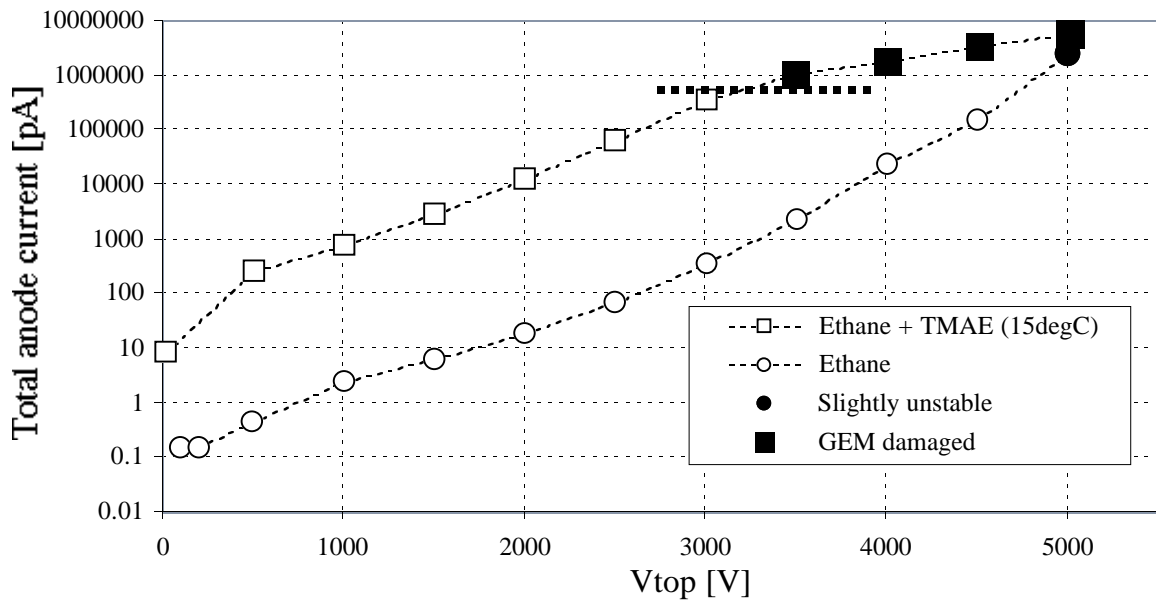


Figure 8. Total anode current for (a) low incident photon flux (open circles) in ethane, corresponding to Fig. 7, and (b) high incident photon flux (open squares) in ethane + TMAE (15°C). In case (a), which was the first one to be measured, the current at $V_{top} = -5\text{kV}$ was showing signs of instability (closed circle), and in case (b), the GEM was damaged at $\sim 3\text{kV}$ (closed squares).

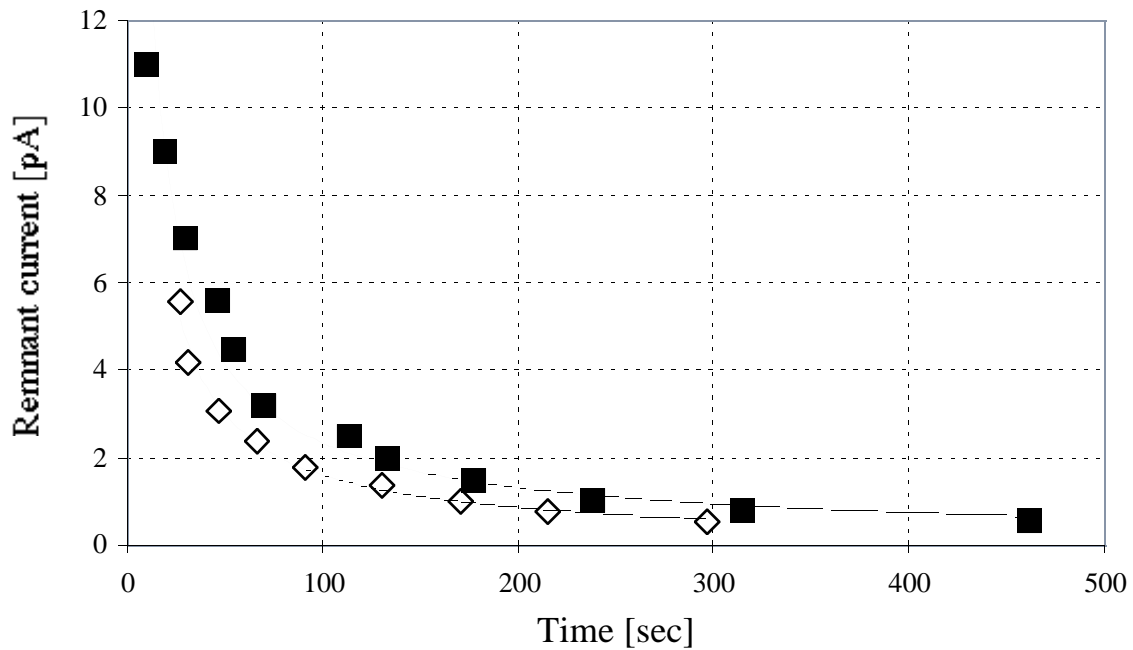


Figure 9. Response of the detector to switching the light off. The voltage was kept constant at either $V_{top} = -4\text{ kV}$ (open diamonds) or $V_{top} = -4.5\text{ kV}$ (black squares). The gas is ethane + TMAE (15°C) at normal pressure and room temperature, and humidity of $\sim 5\text{ppm}$.

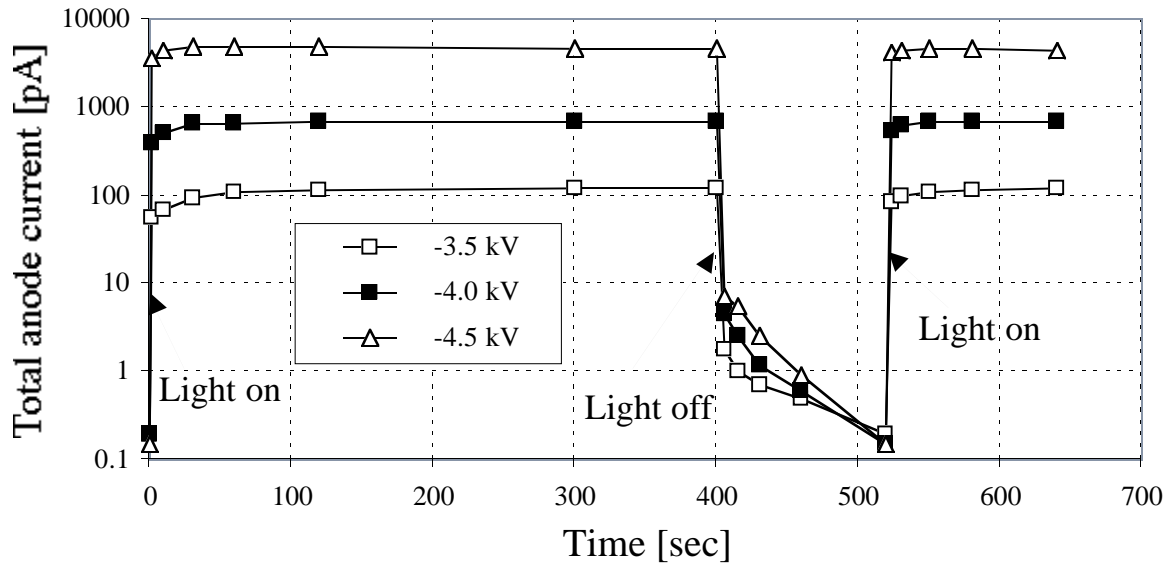


Figure 10. Response of the total anode current to bursts of photon flux at different gas gains, and as a function of time period after the UV lamp shutter opened or closed (the lamp was on continuously). The gas is ethane at normal pressure and room temperature, and humidity of ~5ppm.

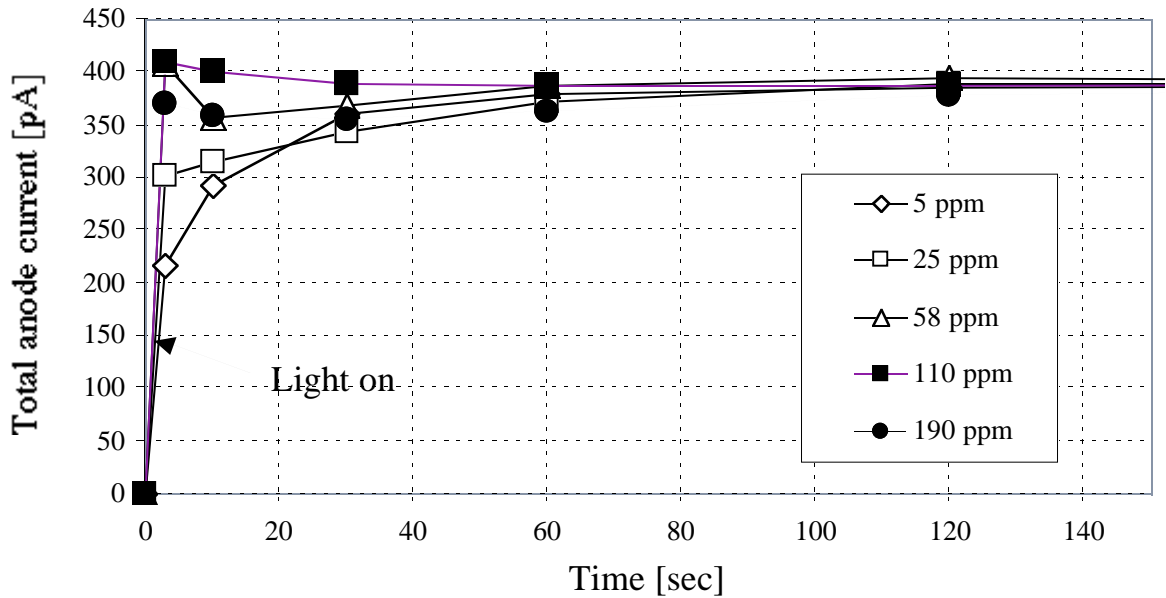


Figure 11. Response of the detector to bursts of photon flux for different humidity levels in ethane. The light burst is controlled by a shutter. The detector voltage V_{top} is 4.0kV.

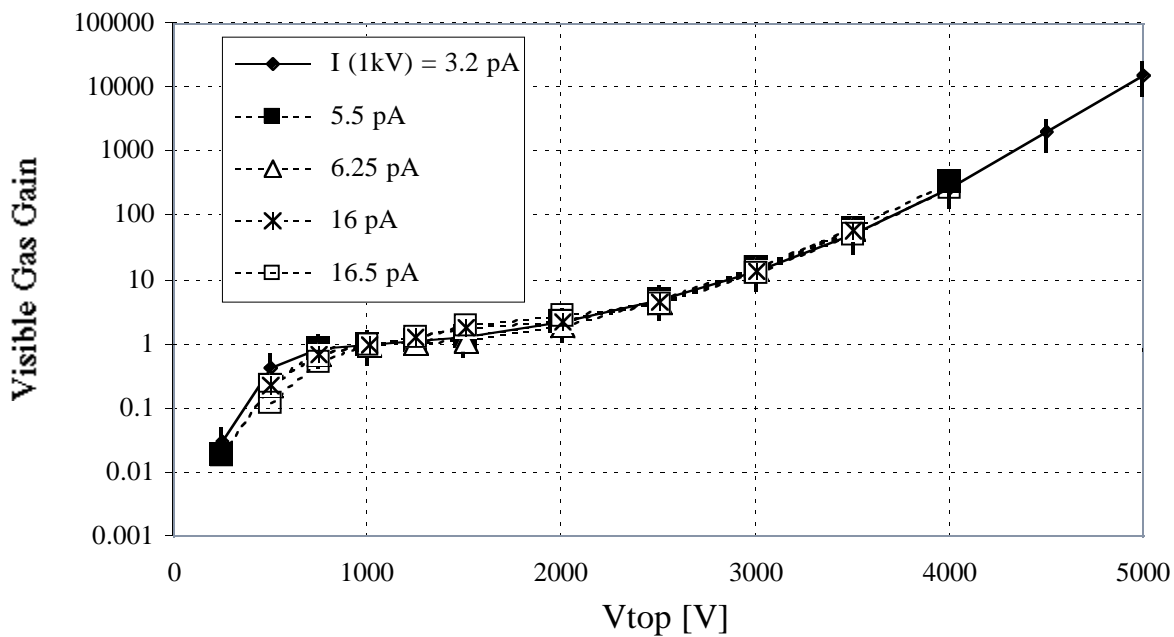


Figure 12. The visible gas gain in ethane + TMAE (15°C) gas at 1 bar as a function of V_{top} , and for several base anode current values measured at $V_{top} = -1$ kV. To determine the anode current density, divide the quoted anode current by the active area of 121.6 mm².